PNAS RESEARCH ARTICLE | PHARMACOLOGY

Allosteric inhibitors targeting the calmodulin-PIP2 interface of SK4 K^+ channels for atrial fibrillation treatment

Shira Burg[a], Shir Shapiro[b], Asher Peretz[a], Elvira Haimov[c], Boris Redko[c], Adva Yeheskel[c], Luba Simhaev[c], Hamutal Engel[c], Avi Raveh[c], Ariel Ben-Bassat[d], Michael Murninkas[b], Rotem Polak[b], Yoni Haitin[d], Yoram Etzion[b,e,1], and Bernard Attali[a,1]

Edited by Ehud Isacoff, University of California, Berkeley, CA; received February 18, 2022; accepted July 05, 2022

The Ca^{2+}-activated SK4 K^+ channel is gated by Ca^{2+}–calmodulin (CaM) and is expressed in immune cells, brain, and heart. A cryoelectron microscopy (cryo-EM) structure of the human SK4 K^+ channel recently revealed four CaM molecules per channel tetramer, where the apo CaM C-lobe and the holo CaM *N*-lobe interact with the proximal carboxyl terminus and the linker S4–S5, respectively, to gate the channel. Here, we show that phosphatidylinositol 4-5 bisphosphate (PIP2) potently activates SK4 channels by docking to the boundary of the CaM-binding domain. An allosteric blocker, BA6b9, was designed to act to the CaM–PIP2-binding domain, a previously untargeted region of SK4 channels, at the interface of the proximal carboxyl terminus and the linker S4–S5. Site-directed mutagenesis, molecular docking, and patch-clamp electrophysiology indicate that BA6b9 inhibits SK4 channels by interacting with two specific residues, Arg191 and His192 in the linker S4–S5, not conserved in SK1–SK3 subunits, thereby conferring selectivity and preventing the Ca^{2+}–CaM *N*-lobe from properly interacting with the channel linker region. Immunohistochemistry of the SK4 channel protein in rat hearts showed a widespread expression in the sarcolemma of atrial myocytes, with a sarcomeric striated Z-band pattern, and a weaker occurrence in the ventricle but a marked incidence at the intercalated discs. BA6b9 significantly prolonged atrial and atrioventricular effective refractory periods in rat isolated hearts and reduced atrial fibrillation induction ex vivo. Our work suggests that inhibition of SK4 K^+ channels by targeting drugs to the CaM–PIP2-binding domain provides a promising anti-arrhythmic therapy.

potassium channel | KCa3.1 | atrial fibrillation | PIP2 | calmodulin

Significance

The SK4 K^+ channel is a member of the family of Ca^{2+}-activated K^+ channels exclusively activated by calcified calmodulin (CaM) and is expressed in immune cells, brain, and heart. Here, we show that phosphatidylinositol 4-5 bisphosphate (PIP2) is a potent activator of human SK4 K^+ channels acting at the interface of the CaM-binding domain. A novel allosteric blocker, BA6b9, was designed to act to the CaM–PIP2-binding domain, a previously untargeted region of SK4 channels. BA6b9 significantly prolonged atrial and atrioventricular effective refractory periods in rat isolated hearts and reduced atrial fibrillation induction ex vivo. Our work suggests that targeting blockers of SK4 K^+ channels to the CaM–PIP2-binding domain provides a promising anti-arrhythmic therapy.

The family of K^+ channels exclusively activated by intracellular Ca^{2+} consists of four members: small-conductance (SK) channels (5–10 pS) comprising three members (SK1–SK3) and one intermediate conductance SK4 channel (20–80 pS) (also called IK or KCa3.1) (1–3). SK4 K^+ channels share the same tetrameric architecture as voltage-gated K^+ channels, where each subunit is endowed with six transmembrane helices (S1–S6) and cytoplasmic *N* and carboxyl termini (2, 3). However, they are exclusively gated by Ca^{2+}-bound calmodulin (CaM), tethered to a CaM-binding domain (CaMBD) located at the proximal carboxyl terminus of the channel and contacting the S4–S5 intracellular linker (2, 3). A recent cryoelectron microscopy (cryo-EM) structure of the human SK4 K^+ channel showed four CaM molecules per channel tetramer (4), where the CaM C-lobe interacts with the proximal carboxyl terminus (helices A and B) in a Ca^{2+}-independent manner. The CaM *N*-lobe interacts in a calcified form with the S4–S5 linker, more specifically with the proximal $S_{45}A$ helix and carboxyl terminus to sense Ca^{2+} and gate the channel (4).

SK4 K^+ channels are expressed in the immune system, such as T cells, B cells, mast cells, macrophages, and microglia (2, 5, 6), as well as in endothelial cells and proliferating neo-intimal smooth muscle cells of the vascular system (7). In immune cells, these channels hyperpolarize the cell membrane and thus favor the driving force for calcium entry, an essential feature for activation, proliferation, and production of cytokines (2, 3, 5, 6). SK4 K^+ channels are also expressed in restricted areas of the brain, such as the hippocampus and cerebellum, where they contribute to the slow afterhyperpolarization (8, 9). We previously identified SK4 K^+ channels in mouse sinoatrial node (SAN) and showed that they are involved in pacemaker activity of cardiomyocytes derived from human embryonic stem cells (10, 11). We and others suggested that SK4 channel blockers may represent an interesting therapeutic approach for treatment of cardiac arrhythmias. Blocking SK4 K^+ channels markedly reduced the occurrence of delayed afterdepolarization and abnormal Ca^{2+} transients following β-adrenergic receptor stimulation in SAN cells from a mouse model of catecholaminergic polymorphic ventricular tachycardia (CPVT) (10). SK4 channel blockage produced PR prolongation in

Author contributions: Y.E. and B.A. designed research; S.B., S.S., A.P., E.H., B.R., A.Y., L.S., H.E., A.R., A.B.-B., M.M., and R.P. performed research; E.H., B.R., A.Y., L.S., H.E., A.R., A.B.-B., and Y.H. contributed new reagents/analytic tools; S.B., S.S., A.P., E.H., B.R., A.Y., L.S., H.E., A.R., A.B.-B., M.M., and R.P. analyzed data; and Y.E. and B.A. wrote the paper.

Competing interest statement: The authors declare a competing interest. There is a pending patent application filed for the new chemical entities disclosed in the manuscript.

This article is a PNAS Direct Submission.

Copyright © 2022 the Author(s). Published by PNAS. This article is distributed under Creative Commons Attribution-NonCommercial-NoDerivatives License 4.0 (CC BY-NC-ND).

[1]To whom correspondence may be addressed. Email: battali@tauex.tau.ac.il or tzion@bgu.ac.il.

This article contains supporting information online at http://www.pnas.org/lookup/suppl/doi:10.1073/pnas.2202926119/-/DCSupplemental.

Published August 15, 2022.

electrocardiogram (ECG) recording and noticeable reduction of arrhythmic features in CPVT model mice at rest and following treadmill exercise (10). SK4 K^+ channels were also shown to abbreviate action potential duration in the canine pulmonary vein myocardium resulting from chronic left atrial volume overload (12). More recently, they were found to be expressed in canine atria and to be up-regulated following acute stroke or rapid atrial pacing in association with atrial effective refractory period (AERP) shortening and increased atrial fibrillation (AF) induction (13, 14). Nonetheless, systematic evaluation of SK4 channels to normal mammalian heart electrophysiology has not been described so far. Moreover, currently existing SK4 channel blockers are essentially targeted to the channel pore and not to the gating machinery.

Here, we show that phosphatidylinositol 4-5 bisphosphate (PIP2) is a potent activator of human SK4 K^+ channels acting at the interface of the CaMBD. We designed an allosteric blocker, BA6b9, targeting the cytosol-facing CaM–PIP2-binding domain (CPBD). This region is located at the boundary of the SK4 channel proximal carboxyl terminus and the S4–S5 linker, which interacts with CaM and PIP2. Docking of BA6b9 onto the human SK4 K^+ channel structure and its functional validation by patch-clamp electrophysiology indicated that BA6b9 inhibits the channel by interacting with two specific residues, Arg191 and His192 in the S4–S5 linker, which are not conserved in SK1–SK3 subunits. This specific interaction confers SK4 channel selectivity and prevents the calcified CaM *N*-lobe from correctly contacting the S4–S5 linker and opening the channel. Immunohistochemistry of the SK4 channel protein in healthy rat hearts showed a prevalent expression in the sarcolemma of atrial myocytes, accompanied by a sarcomeric striated Z-band pattern. The ventricle exhibited a general lower intensity but showed a marked SK4 channel staining at the intercalated discs. BA6b9 significantly prolonged atrial and atrioventricular effective refractory periods in rat isolated hearts and reduced AF induced by carbachol. Overall, our strategy of targeting allosteric inhibitors to the specific CaM–PIP2-binding interface, such as that of SK4 channels, provides the critical advantage of providing a selective target signature and may offer a promising anti-arrhythmic therapy.

Results

PIP2 Is Important for SK4 K^+ Channel Gating. First, we characterized the calcium dependence of the human SK4 K^+ channel in transfected Chinese hamster ovary (CHO) cells using inside-out macropatches. Currents were generated by voltage ramps (−100 mV to +100 mV for 1 s) (Fig. 1 *A* and *B*). Currents were normalized to the maximum response evoked by 3 μM internal free Ca^{2+}, plotted as a function of free Ca^{2+} concentrations, and data points were fitted to a Hill equation, yielding a half-maximal effective concentration (EC_{50}) of 65 nM, a value slightly lower but yet close to that published earlier (15). To examine whether the channel was modulated by PIP2, we cotransfected CHO cells with plasmids encoding SK4 channels

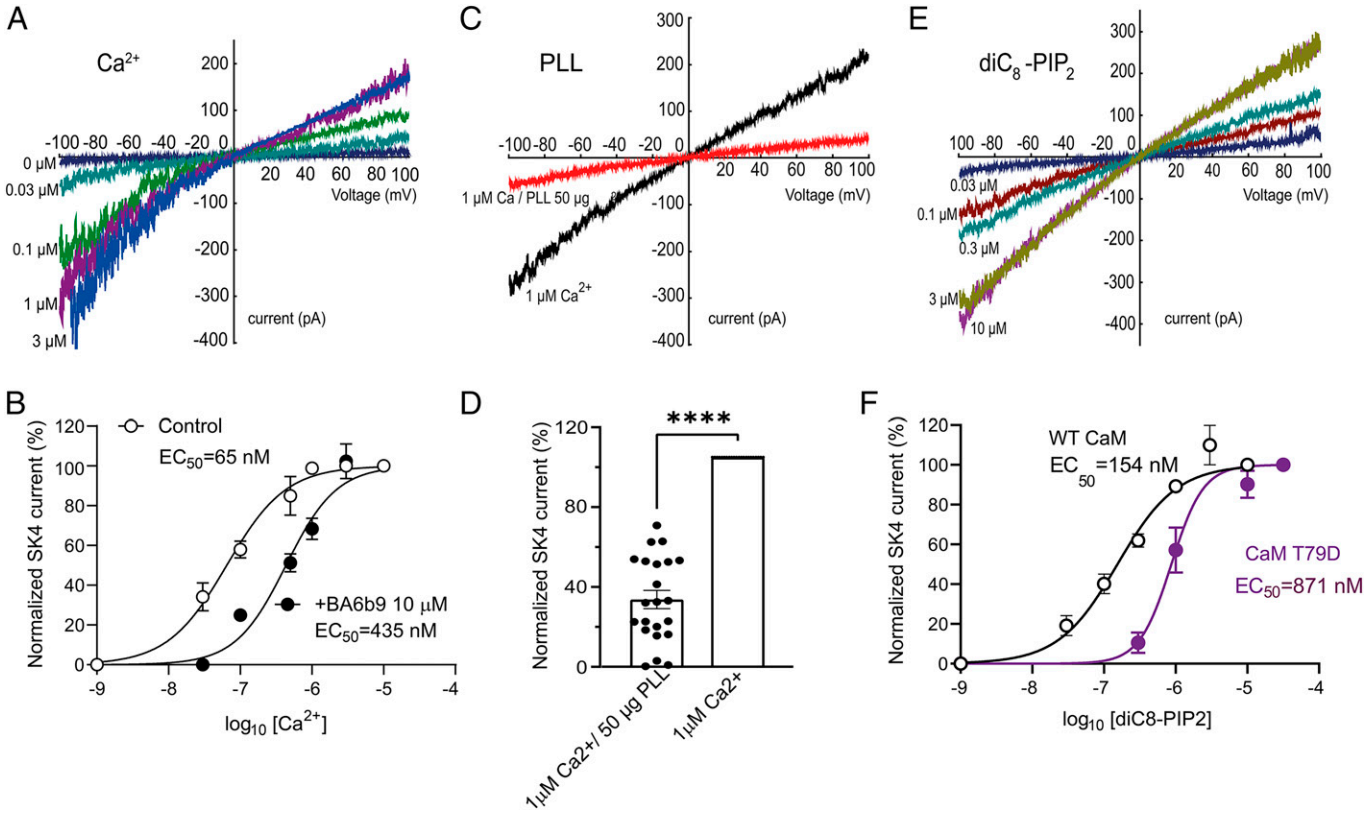

Fig. 1. Inside-out macropatch recordings reveal the importance of calcium and PIP2 for SK4 K^+ channel gating. (*A*) Representative traces of WT SK4 currents recorded from a transfected CHO cell exposed to different intracellular free Ca^{2+} concentrations under inside-out patch-clamp configuration. Currents are recorded by 10 repetitive 1-s-duration voltage ramps from −100 mV to +100 mV from a holding potential of 0 mV. (*B*) Dose-dependent activation of WT SK4 channels by intracellular free Ca^{2+} in the presence (n = 5) and absence (n = 6) of BA69b 10 μM, yielding EC_{50}s of 435 nM and 65 nM, respectively. (*C*) Representative traces of WT SK4 currents before (black) and after PLL (50 μg/mL) internal application (red). (*D*) Internal application of PLL (50 μg/mL) decreases the SK4 current by 68 ∓ 4% (n = 22; two-tailed paired t test, t = 15.71, df = 21, ****P < 0.0001). (*E*) WT SK4 current is enhanced in response to increasing diC8–PIP2 concentrations after prior depletion of endogenous PIP2 by PLL. The experiment is performed with internal 1 μM free Ca^{2+} concentration. (*F*) Dose-dependent activation of WT SK4 channels coexpressed WT CaM (n = 6) or CaM T79D (n = 7) by internal application of diC8-PIP2, yielding EC_{50}s of 154 nM and 871 nM, respectively.

and CaM, which was previously shown to increase channel trafficking to the plasma membrane (16). The currents were recorded from inside-out macropatches, with an intracellular solution containing a saturating concentration of 1 μM free Ca^{2+}. Application of poly-L-lysine (PLL) (50 μg/mL), a well-known PIP2 scavenger (17), caused a rapid and significant decrease in SK4 K^+ currents, with 68% inhibition after 1 min of PLL application (Fig. 1 *C* and *D*), which could not be recovered by increasing intracellular free Ca^{2+} concentrations. In contrast, application of the water-soluble synthetic PIP2 derivative, diC8–PIP2, could significantly and dose-dependently activate the SK4 K^+ currents at 1 μM internal free Ca^{2+} (Fig. 1 *E* and *F*). Normalizing the currents to the maximal activating diC8–PIP2 concentration of 10 μM and fitting the data yielded an EC_{50} of 154 nM, a value of apparent higher affinity than that obtained for wild-type (WT) SK2 channels (1.9 μM) (18). To further confirm the importance of PIP2 in channel activation, CHO cells were cotransfected with plasmids encoding SK4 channels and PIP4,5-kinase that elevates PIP2 levels by producing PIP2 from phosphatidylinositol 4-phosphate (19), and the resulting K^+ currents were recorded in the whole-cell configuration of the patch-clamp technique, in the presence of 1 μM internal free Ca^{2+}. In the presence of PIP4,5-kinase, the current density of WT SK4 channels was considerably increased by 3.7-fold (Fig. 2*A*). Taken together, these data indicate that PIP2 is required for proper SK4 channel gating. However, the high diC8–PIP2 apparent affinity questions how SK4 channels could be properly modulated by PIP2 and Ca^{2+} within a dynamic range of concentrations in physiological conditions. Previous studies showed that phosphorylation of CaM at T79 by casein kinase II (CK2) reduces both the Ca^{2+} and the PIP2 sensitivity of the SK2/CaM channel complex for activation, suggesting that the levels of CaM phosphorylation could modulate the actual affinity of PIP2 and Ca^{2+} for the channel (18, 20). To probe whether phosphorylation of CaM at T79 also affects the activation of SK4 channels by Ca^{2+} and PIP2, we used the phosphomimetic mutant of CaM, T79D. To rule out any effect of CaM on channel trafficking, we first used purified recombinant proteins of WT CaM (3 μM) and CaM T79D (3 μM) that we introduced into the pipette internal solution containing a saturating concentration of 5 μM free Ca^{2+} and recorded the K^+ currents produced by WT SK4 channels. A significant smaller current density (54% decrease) was obtained when the pipette solution contained recombinant CaM T79D (66 pA/pF) as compared with WT CaM (142 pA/pF) (Fig. 2*B*). This is likely due to exchange of the channel-bound endogenous CaM with the

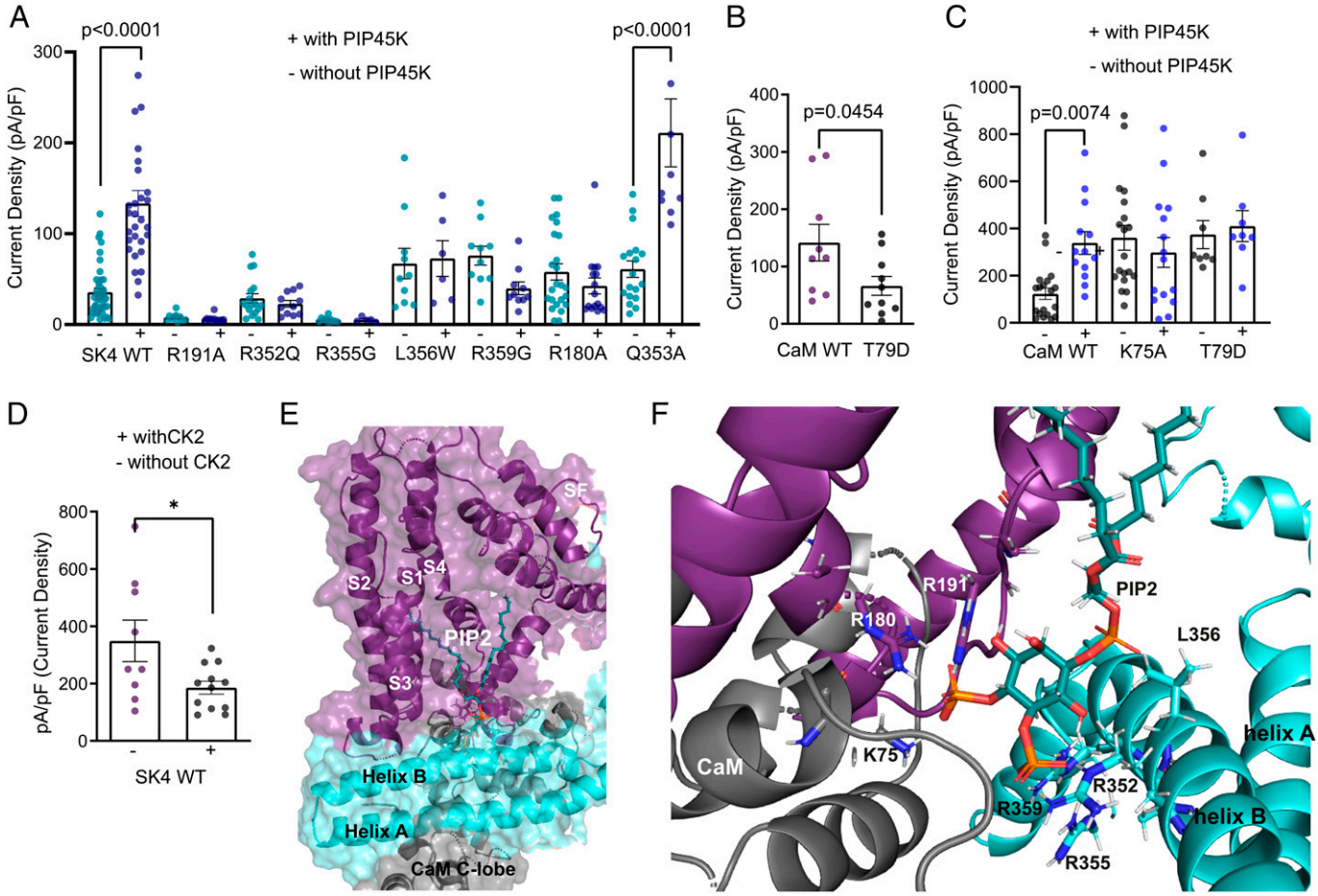

Fig. 2. PIP2–calmodulin interface and SK4 channel activation. (*A*) Effects of increased PIP2 levels by cotransfection with PIP4,5 kinase on WT and mutant SK4 channels. Whole-cell SK4 K^+ currents are activated using a voltage ramp protocol from −100 mV to +60 mV for 150 ms. PIP4,5 kinase significantly increases WT SK4 and mutant Q353A currents by 3.7- and 3.5-fold, respectively (n = 41 and n = 29, respectively; one-way ANOVA, F (15, 224) = 17.74, Sidak's multiple comparisons test $P < 0.0001$); all other mutants are not activated by PIP4,5 kinase (n = 5–36). (*B*) Internal purified CaM T79D (3 μM) produces significantly lower SK4 currents than with WT CaM (n = 10–11, two-tailed unpaired t test, t = 2.099, df = 19, $P < 0.0454$). (*C*) PIP4,5 kinase significantly increases SK4 currents cotransfected with WT CaM, while no effects are observed with CaM mutants K75A and T79D (n = 8–19). (*D*) Cotransfection of WT SK4 channels with CK2α subunit enzyme significantly decreases current density by 47 ∓ 6% (n = 9–12, two-tailed unpaired t test, t = 2.433, df = 19, $^*P = 0.0250$). (*E*) Docking of PIP2 (cyan/orange stick) to the Ca^{2+}-bound state I (6CNN) of the SK4 channel cryo-EM structure; the S1–S4 helices, the CaM, and the SK4 proximal carboxyl terminus (helices A and B) are shown in deep purple, gray, and light cyan, respectively. (*F*) Zoom-in of the PIP2-binding pocket showing the interacting residues.

CaM T79D mutant. Similarly, coexpression of WT SK4 channels with the CK2 α subunit enzyme, known to phosphorylate CaM at T79, produced a 47% decrease of the current density with a pipette solution containing 5 μM free Ca^{2+} and 5 mM ATP K_2 (Fig. 2*D*). Then, we examined the ability of PIP2 to stimulate SK4 currents under conditions of CaM phosphorylation. We coexpressed WT SK4 channels with either WT CaM or CaM T79D in the absence or presence of PIP4,5-kinase. In the presence of PIP4,5-kinase, the current density of WT SK4 channels was significantly increased upon coexpression with WT CaM (2.6-fold), but not with CaM T79D (1.1-fold) (Fig. 2*C*). Finally, we measured in inside-out macropatches the apparent affinity of diC8–PIP2 for WT SK4 channel activation in the presence of the phosphomimetic mutant CaM T79D. We found that diC8–PIP2 exhibits a 5.6-fold lower affinity with CaM T79D (EC_{50} = 871 nM) than with WT CaM (EC_{50} = 154 nM) (Fig. 1*F*). Altogether, these data suggest that, like with SK2 channels (18, 20), phosphorylation of CaM at T79 can lower the sensitivity of SK4 channel activation by PIP2 and Ca^{2+}.

PIP2 Molecular Docking and Experimental Validation. The PIP2 molecule bears a net negative charge at physiological pH that allows it to engage in electrostatic interactions with positively charged regions of proteins. The human SK4 channel cryo-EM structure (4) was previously determined in the absence of PIP2. Therefore, using the Glide docking algorithm (see *Materials and Methods*), PIP2 was docked to the Ca^{2+}-bound state I (6CNN) of the channel at the interface of CaM and the SK4 proximal carboxyl terminus with CaM T79 serving as an anchor. More than 100 docking simulations were performed and scored based on their docked binding energies, where the final PIP2 docking pose was selected according to the best energy score. Molecular docking of PIP2 revealed that the outward-facing fatty acid tail could fit into a gorge formed by the boundaries of S1, S2, S3, and S4 transmembrane helices (Fig. 2*E*). The inward-facing phosphate head groups are near the bottom of the PIP2-binding pocket formed by linker S4–S5, the CaM interlobe region, and helix B of the proximal carboxyl terminus from an adjacent subunit (Fig. 2*E*). In linker S4–S5, the guanidinium group of R180 could interact via H-bonding with the phosphate P4 of PIP2 (distance H–O = 1.7 Å). Similarly, R191 can be engaged via its guanidinium functionality into H-bonding with the P4 of PIP2 (distance H–O = 2.0 Å) (Fig. 2*F*). In helix B of the neighboring subunit, thanks to their guanidinium groups, R352, R355, and R359 could interact via H-bonding with the phosphate P5 of PIP2 (distances H–O = 1.7 Å, 2 Å, and 2.5 Å, respectively). In the same region, the nonpolar residue L356 is close to the PIP2 phosphodiester moiety (distance H–O = 2.7 Å), and we assume that hydrophobic interactions may affect the positioning of the fatty acid tail in the gorge. In the CaM interlobe linker, the ε amine of K75 can interact via H-bonding with the phosphate P4 of PIP2 (distance H–O = 1.8 Å) (Fig. 2*F*).

To validate functionally the PIP2 docking site, we mutated positively charged residues interacting with the oxygen of the PIP2 phosphate head groups as well as other residues that were at putative atomic proximity of the PIP2 molecule, such as L356 in helix B. We measured the impact of the mutations on the current densities resulting from coexpression of SK4 channels with PIP4,5-kinase using whole-cell patch-clamp recording, with 1 μM free Ca^{2+} in the pipette solution (Fig. 2 *A* and *C*). Mutants R180A, R191A of linker S4–S5 and R352Q, R355G, R359G of helix B, which lack positive charge, were unable to be activated by PIP4,5-kinase (1.6-, 0.8-, 0.8-, 1-, and 0.5-fold, respectively) as compared with WT SK4 (3.7-fold) (Fig. 2*A*). Mutant K75A of the CaM linker coexpressed with WT SK4 channel was also unable to be activated by PIP4,5-kinase (0.7-fold) (Fig. 2*C*). Mutant L356W of helix B is insensitive to activation by PIP4,5-kinase (1.1-fold), suggesting that this residue, in proximity to the PIP2 phosphodiester bond, may play a role in the appropriate PIP2 docking into the gorge of the S1–S4 transmembrane region. Noteworthy, mutation of residue Q353 (Q353A), which does not interact with PIP2 and is the close neighbor of residue R352, is potently activated by PIP4,5-kinase (3.5-fold) (Fig. 2*A*), underscoring the specificity of PIP2 interactions. In all, these data suggest that PIP2 is a pivotal gating molecule sitting in a pocket formed by S1–S4 helices, linker S4–S5, CaM interlobe region, and helix B of the proximal carboxyl terminus of the neighboring subunit.

Design of Small Allosteric Inhibitors Targeting the CPBD. The currently existing SK4 channel blockers (e.g., TRAM34 or clotrimazole) act on the channel pore and may not be suitable for clinical development so far (21, 22). In this work, we aimed to target inhibitors to the SK4 channel gating domain. We designed new compounds, 2-benzimidazolinone derivatives, based on the prototypical opener 1-EBIO (23) (Fig. 3*A*), which was previously shown to interact at the interface of the CaM *N*-lobe and the CaM-binding domain of the proximal carboxyl terminus of SK2 channels (18, 24, 25) (*SI Appendix*, Fig. S1*A*). We first substituted halogen atoms (chloride or bromide) on the aromatic ring of the benzimidazole moiety and obtained compounds such as BA40 and BA100, which were not blockers but rather weak openers of SK4 channels with 1.4-fold and 1.3-fold current increase, respectively, at 10 μM (*SI Appendix*, Fig. S1 and Fig. 3 *B* and *D*). Next, we designed 2-benzimidazolinone analogs with one or two linear alkyl chains of various lengths from 1 to up to 12 carbons (*SI Appendix*, Fig. S1). Out of 45 synthesized molecules, all derivatives with two linear alkyl chains of various lengths were inactive on SK4 channels. Among 2-benzimidazolinone derivatives bearing only one linear alkyl chain, blockers of SK4 channels were obtained only with analogs comprising alkyl chains of 5–7 carbons, such as BA4b, BA5b, and BA6b (*SI Appendix*, Fig. S1). BA6b, which exhibits a heptyl chain, significantly inhibited SK4 currents by 25% and 50% at 20 μM and 50 μM, respectively (Fig. 3 *C* and *D*). Interestingly, analogs bearing linear alkyl chains of less than five and more than eight carbons were inactive on SK4 channels (*SI Appendix*). To improve the activity of BA6b, we designed a 2-benzoxazolinone analog, BA6b9, comprising a benzoxazole ring bearing a carbonyl group and a linear heptyl tail connected to the benzoxazole nitrogen. We obtained the actual most potent compound, which reversibly blocked the SK4 currents with an apparent half-maximal inhibitory concentration (IC_{50}) of 8.6 μM (Fig. 3 *E* and *F*, see also *SI Appendix*, Fig. S2). In inside-out macropatches (Fig. 3*G*), 10 μM BA6b9 potently inhibits the SK4 currents by 66%. In view of its hydrophobic alkyl tail, the apparent affinity of BA6b9 is likely underestimated, knowing its low solubility in aqueous solutions and its potential propensity to form micellar aggregates. We performed a solubility assay where a 10-mM stock solution of BA6b9 in DMSO was diluted to 0.5 mM in PBS, shaken in room temperature for 1.5 h, and then diluted to a 250-μM solution using a mobile phase mixture and injected to high-performance liquid chromatography (HPLC). Knowing the retention time of BA6b9, we could quantify and compare the peak area of a 250-μM DMSO solution (100% DMSO) and a 250-μM DMSO/PBS solution (5% DMSO). The solubility of BA6b9 in the DMSO/PBS solution was ∼6 μM, meaning that the actual IC_{50} of BA6b9 is likely overestimated and might be closer to 0.2 μM.

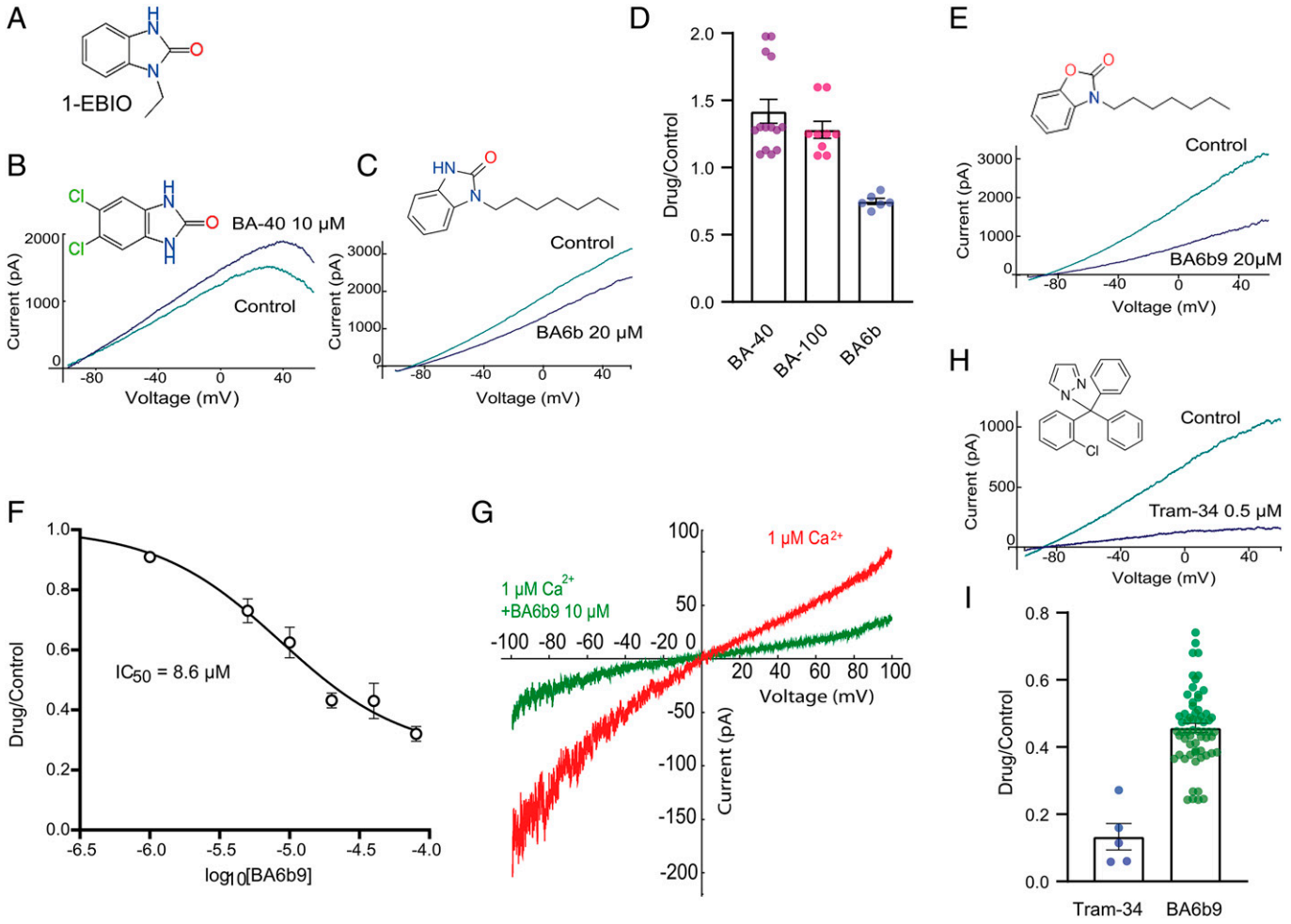

Fig. 3. Effects of small allosteric modulators on SK4 channel activation. (*A*) Chemical structure of 1-EBIO. (*B*) Representative trace of WT SK4 currents in the absence and presence of 10 μM BA-40, showing activation of ~1.4-fold. Whole-cell SK4 K^+ currents are activated using a voltage ramp protocol from −100 mV to +60 mV for 150 ms. (*C*) Representative trace of WT SK4 currents in the absence and presence of 20 μM BA6b, showing an inhibition of ~25%. (*D*) Statistical summary of the pharmacological effects of 10 μM BA-40, 10 μM BA-100, and 20 μM BA6b on WT SK4 currents with 42 ∓ 8% activation (n = 14), 28 ∓ 6% activation (n = 9), and 25 ∓ 2% inhibition (n = 6), respectively. (*E*) Representative trace of WT SK4 currents in the absence and presence of 20 μM BA6b9, displaying an inhibition of ~56%. (*F*) Dose-dependent inhibition of WT SK4 channels by BA69b yielding an apparent IC_{50} of 8.6 ∓ 0.8 μM (n = 6). (*G*) Representative traces of an inside-out macropatch from a CHO cell expressing WT SK4 channels in the absence and presence of 10 μM BA6b9 under internal 1 μM free Ca^{2+} concentration. Currents are recorded by 10 repetitive 1-s-duration voltage ramps from −100 mV to +100 mV from a holding potential of 0 mV. (*H*) Representative trace of WT SK4 currents in the absence and presence of 0.5 μM Tram-34, demonstrating an inhibition of ~86%. (I) Statistical summary of the pharmacological effects of 0.5 μM Tram-34 and 20 μM BA6b9 on WT SK4 currents with 86 ∓ 4% (n = 5) and 56 ∓ 1% (n = 41) inhibition, respectively.

However, in this study, we stuck to the nominal concentrations of all drugs for the sake of clarity and systematically worked with filtered solutions (0.2 μm Whatman filter) containing 0.1% DMSO. Although BA6b9 is a weaker blocker of SK4 channels when compared with Tram-34, it acts to a different region of SK4 channels (see below) (Fig. 3 *E–I*; 0.5 μM Tram-34 and 20 μM BA6b9 produced 87% and 56% inhibition, respectively).

BA6b9 Molecular Docking and Experimental Validation. Molecular docking of BA6b9 to the Ca^{2+}-bound state I (6CNN) of the SK4 channel was performed in the presence of bound PIP2 that was docked as described above. The docking pose revealed that the molecule fits into a gorge formed by boundaries of S1 and S4 transmembrane helices and linker S4–S5 near to the bound PIP2, where the inward-facing heptyl tail contacts the bottom of the BA6b9-binding pocket formed by the CaM linker (Fig. 4*F*). In linker S4–S5, the guanidinium group of R191 could interact via H-bonding with the carbonyl oxygen from the benzoxazole group of BA6b9 (distance H–O = 1.9 Å) (Fig. 4*F*). Residue H192 can engage into aromatic H-bonding or π–π stacking interactions between the imidazole moiety of histidine and the benzoxazole ring of BA6b9 (d= 4.2 Å). In the docking pose, residue M76 of the CaM linker "clashes" with BA6b9, while M72 might be involved in hydrophobic interactions (Fig. 4*F*). Molecular docking of 1-EBIO and BA40 to the SK4 channel (6CNN) reveals that both openers dock very differently from BA6b9. In contrast to BA6b9, 1-EBIO and BA40 are distant from the CaM residue M76 (d >11Å) and thereby do not clash with it in the computational docking (*SI Appendix*, Fig. S3). Both molecules sit in a similar way at the bottom of the inward-facing phosphate head groups of PIP2, and their docking poses suggest that they might stabilize the SK4 channel–CaM complex by interacting with the CaM interlobe linker (R74, K75) (*SI Appendix*, Fig. S3).

To validate functionally the ligand docking site, we mutated residues that are expected to interact with BA6b9, such as R191 and H192 of linker S4–S5, M72 and M76 of the CaM linker, and other residues that are more distant from BA6b9 as negative control. Mutations of residues in linker S4–S5, such as Y179S, S181A, A184R, Q187A, and R189A, which are remote from the docked ligand, exhibited comparable inhibition by 20 μM BA6b9 to that of WT SK4 channels (ranging from

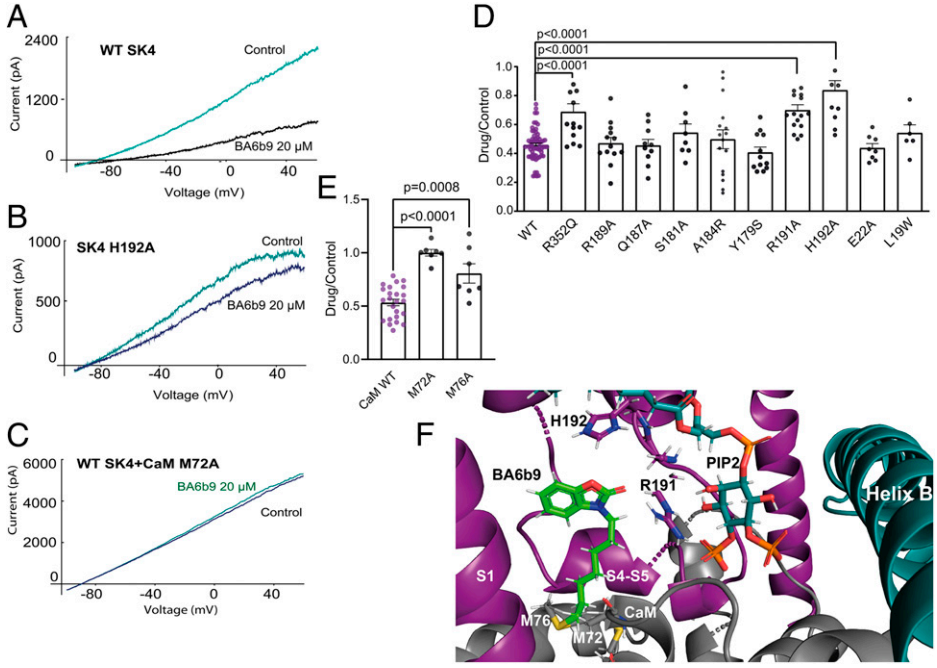

Fig. 4. Molecular docking of BA6b9 and functional validation in transfected CHO cells. (*A*) Representative trace of WT SK4 currents in the absence and presence of 20 μM BA6b9. (*B*) Representative trace of the SK4 mutant H192A current in the absence and presence of 20 μM BA6b9, showing the significant lower inhibition (16%) compared with that obtained for WT SK4 (56%). (*C*) Representative trace of WT SK4 channel cotransfected with CaM mutant M72A in the absence and presence of 20 μM BA6b9, showing complete insensitivity to inhibition by BA6b9. (*D*) SK4 channel mutants R352Q, R191A, and H192A are significantly less sensitive to the inhibitory effect of 20 μM BA6b9 compared with WT SK4 (one-way ANOVA, F (10, 165) = 10.27; Dunnett's multiple comparisons test; $n = 14$, $P < 0.0003$, $n = 16$, $P < 0.0001$ and $n = 11$, $P < 0.0001$, and $n = 62$, respectively). (*E*) Statistical summary of the pharmacological effects of 20 μM BA6b9 on WT SK4 channel cotransfected with CaM mutants M72A and M76A, displaying their significant lower sensitivity to BA6b9 inhibition (one-way ANOVA, F(2, 35) = 25.59, Dunnett's multiple comparisons test; respectively, 0 ∓ 3% inhibition $n = 7$, $P < 0.0001$ and 19 ∓ 9% inhibition $n = 7$, $P = 0.0008$) as compared with WT CaM (47% inhibition, $n = 24$). (*F*) BA6b9-binding pocket showing the interacting residues. BA6b9 is docked to the Ca^{2+}-bound state I (6CNN) of the SK4 channel cryo-EM structure; BA6b9, PIP2, S1 helix and S4–S5 linker, CaM, and the SK4 proximal carboxyl terminus (helix B) are represented by green stick, cyan/orange stick, deep purple, gray, and cyan, respectively.

59 to 46% inhibition) (Fig. 4 *D* and *F*). Mutants located at the N terminus, such as L19W and E22A, do not interact with BA6b9 yet showed 46% and 56% inhibition, respectively, similar to that obtained with WT (56%). In contrast, mutant residues interacting with BA6b9, such as R191A and H192A, displayed significantly weaker inhibition of 30% and 16%, respectively, as compared with WT (Fig. 4 *A*, *B*, *D*, and *F*). Importantly, these two residues, Arg191 and His192, are specific to SK4 channels and are replaced, respectively, by Asn and Thr in SK1, SK2, and SK3 channels (*SI Appendix*, Fig. S4). Therefore, it was important to examine the effect of BA6b9 on the SK1–3 homomeric channels. While 20 μM BA6b9 produced a 56% inhibition of WT SK4 currents, it did not affect SK1, SK2, and SK3 currents with a drug/control current ratio of 1.18, 1.34, and 0.95, respectively (*SI Appendix*, Fig. S4). Interestingly, mutant R352Q of helix B, which is distant from BA6b9 and is unable to be activated by PIP4,5-kinase (Fig. 2*A*), showed a significant smaller inhibition (31%) compared with WT, suggesting an allosteric impact of this helix B site to the docking stability of the ligand (Fig. 4*D*). In the CaM linker, which forms the floor of the BA6b9-binding pocket, mutants M72A and M76A exhibited no or weak inhibition of 0% and 19%, respectively, suggesting that, under these conditions, the CaM mutants do not clash with BA6b9, which allows the correct CaM interaction with linker S4–S5 and precludes the blocking effect of BA6b9 (Fig. 4 *C*, *E*, and *F*). Thus, we assume that BA6b9 exerts its inhibitory action by preventing the calcified CaM *N*-lobe to properly contact its S4–S5 linker site to open the channel, which is expected to affect the Ca^{2+} dependence of SK4 channels. To probe the postulated allosteric inhibition of BA6b9, we measured the Ca^{2+}-dependent activation of WT SK4 channels in inside-out macropatches in the absence and presence of 10 μM BA6b9. We found that BA6b9 lowers the sensitivity of SK4 channels to Ca^{2+} by about sevenfold with an EC_{50} for Ca^{2+} of 435 nM (Fig. 1*B*). As our purposed goal was to target this allosteric blocker to SK4 channels in the heart, it was important to examine its selectivity to other prominent cardiac K^+ currents, such as I_{Kur} (Kv1.5), $I_{K,slow}$ (Kv2.1), I_{Kr} (Kv11.1 or *hERG*), and *IKs* (KCNQ1+KCNE1) (26–28). Results indicate that none of these K^+ channels were affected by BA6b9 in transfected CHO cells (*SI Appendix*, Fig. S4 *B* and *D*).

Expression of the SK4 Channel Protein in Adult Rat Hearts. In view of our previous work (10, 11) and other recent studies (12–14, 29) suggesting that SK4 channel blockers may improve heart rhythm in cardiac arrhythmias, we examined the expression of SK4 channels in adult healthy rat hearts by immunohistochemistry. Before immunostaining of the cardiac tissue, three different antibodies were first tested for their specificity by their ability to label the SK4 channel expressed in transfected CHO cells. Using nontransfected cells as a measure of background staining and SK4-transfected cells as a positive control, only one antibody (sc-365265, Santa Cruz) demonstrated excellent label selectivity (*SI Appendix*, Fig. S5). Indeed, this antibody was very selective for SK4 channels, since it did not label SK1-, SK2-, and SK3-transfected CHO cells as well as nontransfected CHO cells (*SI Appendix*, Fig. S5). Immuno-localization of SK4 channels was performed on 4-μm-thick slices of left atrium and ventricles. We found a widespread expression of the SK4 channel protein in atrial myocytes, with a staining at the sarcolemma as well as the intracellular membrane network with a sarcomeric striated Z-band pattern, illustrated by the colabel of

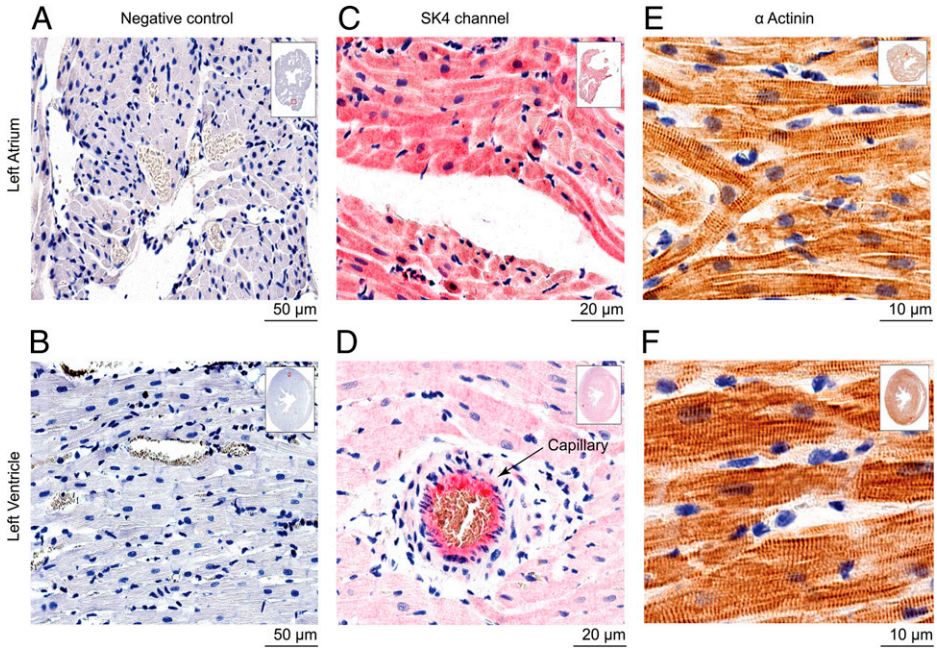

Fig. 5. Immunohistochemistry of SK4 channel and α-actinin expression in healthy rat cardiac tissue. Representative left atrial (LA) and left ventricular (LV) paraffin embedded sections of a healthy rat heart. (*A* and *B*) Sections are processed and stained with secondary antibodies as a negative control. (*C* and *D*) Sections are labeled exclusively with SK4 monoclonal antibody and stained with Congo Red as described in "*Materials and Methods*". Note the enhanced intensity and scatter of the red staining in the LA cardiomyocytes in (*C*) compared with the LV in (*D*). Note also, in (*D*), the positive staining of SK4 channel of a blood vessel. (*E* and *F*) Sections are exclusively labeled with α-actinin polyclonal antibody and stained with 3,3′-diaminobenzidine as described in "*Materials and Methods*". Notice the sarcomeric striated Z-band pattern of α-actinin.

α-actinin (Figs. 5 *C* and *E* and 6 *A* and *B*). In the ventricle, SK4 channel staining showed a lower overall intensity compared with the atrial tissue, especially considering the marked staining in vascular endothelium where SK4 is abundantly present (Fig. 5*D*). Staining was evident not only in the sarcolemma and striations across cells but was additionally localized at the intercalated discs between ventricular myocytes (Fig. 6 *C* and *D*). Importantly, immuno-localization of SK4 channel was detected in slices of human heart with a stronger staining of the atrium than the ventricle. Also, similar to rat heart, a marked SK4 channel expression was found in the vascular endothelium of atrial and ventricular capillaries (*SI Appendix*, Fig. S6).

Effects of BA6b9 on Isolated Rat Heart Preparations. To examine the impact of BA6b9 on cardiac electrophysiology and mechanical function, we used the Langendorff isolated heart

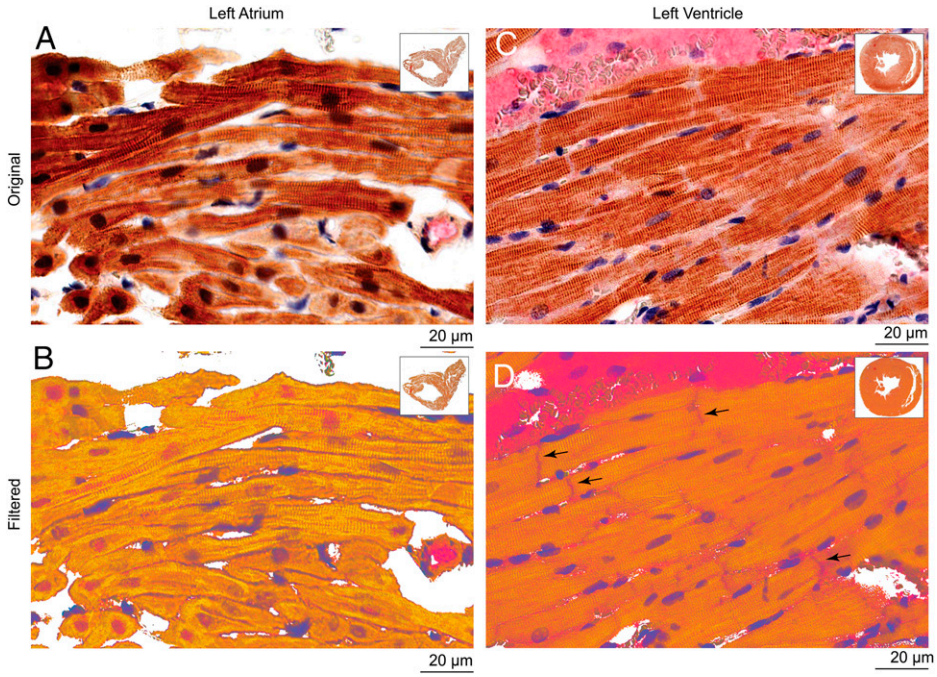

Fig. 6. Double staining immunohistochemistry of SK4 channel and α-actinin expression in healthy rat cardiac tissue. (*A* and *B*) Double-stained LA with SK4 channel and α-actinin antibodies, showing SK4 channel localization at the sarcolemma as well as in the intracellular membrane network with a sarcomeric striated Z-band pattern in (*B*). (*C* and *D*) Double-stained LV with SK4 channel and α-actinin antibodies showing localization not only in the sarcolemma and striations across the cells but also at the intercalated discs between ventricular myocytes in (*D*) (black arrows).

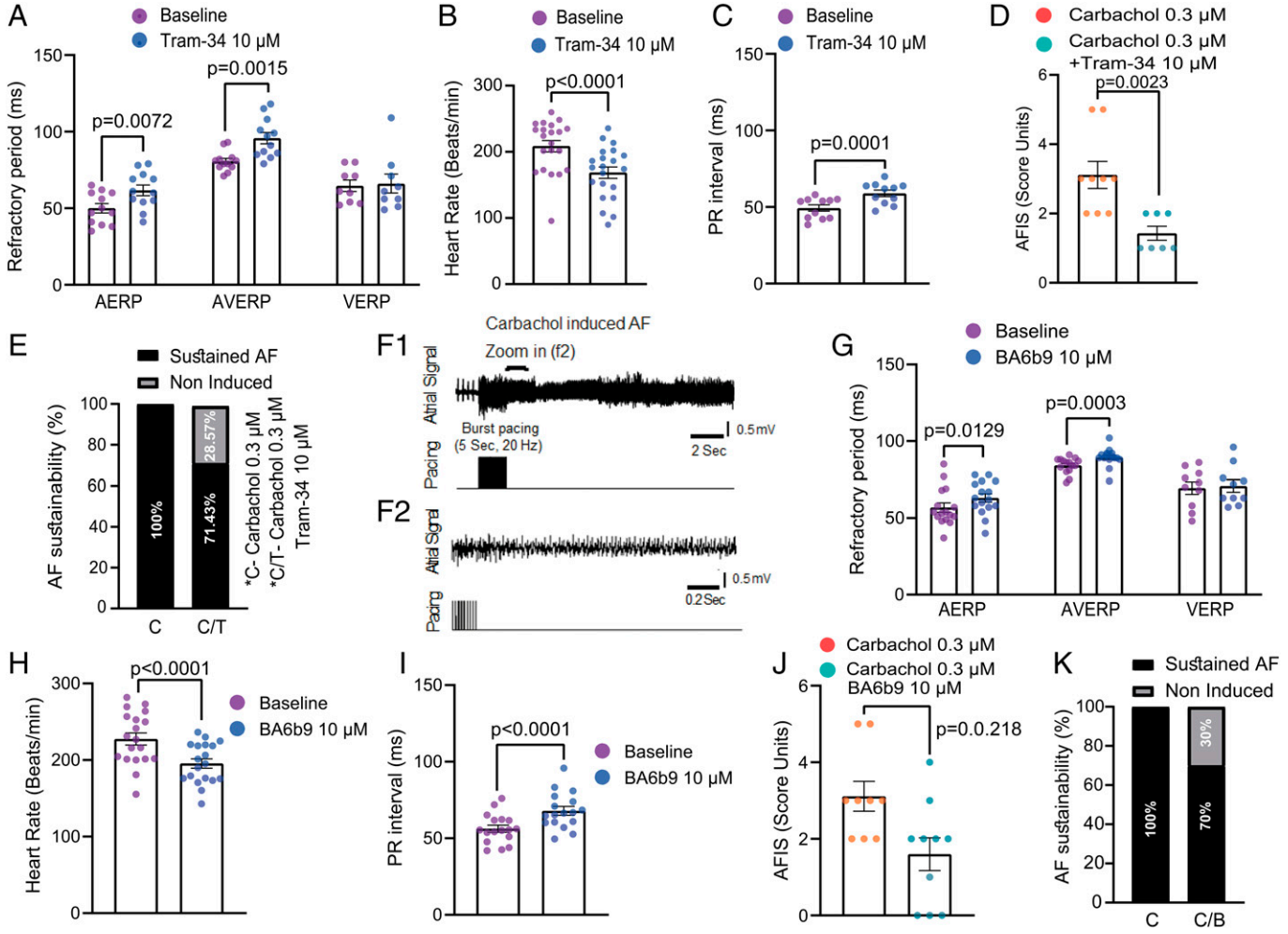

Fig. 7. Tram-34 and BA6b9 effects on the electrophysiological properties of the isolated rat hearts. Data are analyzed by two-tailed paired *t* test, except in (*D*) and (*J*), by two-tailed Mann Whitney test. (*A* and *G*) AERP and AVERP are significantly prolonged by 10 μM Tram-34 (n = 12, t = 3.293, df = 11, P = 0.0072 and t = 4.197, df = 11, P = 0.0015, respectively) and 10 μM BA6b9 (n = 16, t = 2.822, df = 15, P = 0.0129 and n = 15, t = 4.706, df = 14, P = 0.0003, respectively). (*B* and *H*) Heart rate is significantly decreased by 10 μM Tram-34 (n = 21, t = 5.816, df = 20, P < 0.0001) and 10 μM BA6b9 (n = 19, t = 6.209, df = 18, P < 0.0001). (*C* and *I*) PR interval is significantly increased by 10 μM Tram-34 (n = 11, t = 5.997, df = 10, P = 0.0001) and 10 μM BA6b9 (n = 17, t = 5.592, df = 16, P < 0.0001). (*D* and *J*) Ten micromolar Tram-34 and 10 μM BA6b9 significantly lower AFIS (see *Materials and Methods*) by 54% and 48%, respectively, compared with carbachol alone (n = 7, P = 0.0023 and n = 10, P = 0.0218, respectively). (*E* and *K*) Ten micromolar Tram-34 and 10 μM BA6b9 prevent sustainability (see *Materials and Methods*) in 28% (2/7) and 30% (3/10) of heart preparations, respectively. (*F1*) Representative recording showing AF induced after 10-min incubation with 0.3 μM carbachol by burst pacing through a quadripolar electrode attached to the high right atrium. (*F2*) Higher time resolution recording of the area marked by horizontal bar in (*F1*).

model in adult healthy rats. As a proof of concept, we first used Tram-34, a prototypical SK4 channel blocker (30). Tram-34 (10 μM) produced significant prolongation of AERP and atrioventricular node effective refractory period (AVERP) without affecting the ventricular effective refractory period (VERP) (Fig. 7*A*). Tram-34 induced negative chronotropic and dromotropic effects reflected by the reduced heart rate and prolonged PR interval (Fig. 7 *B* and *C*). Likewise, BA6b9 (10 μM) prolonged AERP and AVERP but did not change the VERP (Fig. 7*G* and *SI Appendix*, Fig. S7). Also, BA6b9 produced similar chronotropic and dromotropic effects (Fig. 7 *H* and *I*). Neither BA6b9 nor Tram-34 affected the diastolic capture threshold in atria or ventricles. Importantly, BA6b9 (10 μM) and Tram-34 (10 μM) can decrease the AF substrate induced by the cholinergic agonist carbachol (0.3 μM) (Fig. 7 *D*, *F*, *J*, and *K*). Sustained AF was induced using a burst pacing protocol in which pacing intensity is gradually increased from 2× to 6× diastolic threshold. While 100% AF induction was obtained with carbachol (0.3 μM) alone, only 71% and 70% AF induction were achieved when Tram34 or BA6b9 were present (Fig. 7 *E* and *K*). Moreover, when we quantified sustained induction by an AF induction score (AFIS), where the lower the induction threshold the higher is the score, Tram-34 and BA6b9 markedly reduced the AFIS from 3.1 (carbachol alone) to 1.4 and 1.6, respectively (Fig. 7 *D* and *J*). Regarding the hemodynamic parameters, Tram-34 did not affect the left ventricular developed pressure (*SI Appendix*, Fig. S8*A*) but mildly affected the contraction kinetics (*SI Appendix*, Fig. S8 *B* and *C*). BA6b9 slightly reduced the developed pressure and tended to affect the contraction kinetics in a similar manner as Tram-34 (*SI Appendix*, Fig. S8 *E–G*). While Tram-34 mildly lowered the coronary flow under constant perfusion pressure, indicating an increase in coronary resistance, BA6b9 had no such effect (*SI Appendix*, Fig. S8 *D* and *H*).

Discussion

In this study, we revealed four important new findings: (1) we showed that PIP2 is a potent activator of SK4 K^+ channels and characterized its molecular binding pocket; (2) we designed a novel allosteric blocker, BA6b9, acting to a previously untargeted

region of SK4 channels, the CPBD; and (3) immunohistochemistry of the SK4 channel protein in adult healthy rat hearts showed a widespread expression in the sarcolemma of atrial myocytes, accompanied by a sarcomeric striated Z-band pattern. The ventricle exhibited a general lower intensity but showed a marked SK4 channel staining at the intercalated discs. (4) We found that SK4 channel blockade increases atrial and atrioventricular refractoriness, suggesting that targeting the CPBD region by allosteric inhibitors can offer a novel promising anti-arrhythmic therapy.

Several lines of evidence indicate that PIP2 is important for SK4 channel gating: (1) low concentration of PLL (50 μg/mL) produces rapid inhibition of SK4 currents and (2) the PIP2 derivative, diC8-PIP2, dose-dependently activates SK4 currents in the presence of Ca^{2+}. (3) PIP4,5-kinase that elevates PIP2 levels (19) markedly increases the current density of SK4 channels. Although the recent cryo-EM structure of the human SK4 channel was determined in the absence of PIP2 molecules (4), our docking and electrophysiology validation data suggest that PIP2 plausibly binds to a pocket where the outward-facing fatty acid tail accommodates to the gorge molded by boundaries of transmembrane helices S1–S4, while the inward-facing phosphate head groups interact via H-bonding with linker S4–S5, CaM interlobe region, and helix B of the proximal carboxyl terminus from an adjacent subunit. This PIP2 site is part of the gating machinery, where it could exert in cooperation with Ca^{2+}–CaM its gating function. PIP2 may assist the downward pulling of linker S4–S5 and, by its interaction with helix B of the neighboring subunit, may help to expand S6 helices and couple the linker movement initiated by the calcified CaM *N*-lobe to open the remote channel gate. We do not exclude the possibility that additional PIP2 molecules interact with other regions of the channel. (4) PLL inhibitory effects could not be reversed by increases in intracellular Ca^{2+} but only by simultaneous application of both Ca^{2+} and diC8-PIP2. The crucial requirement of PIP2 for SK4 channel gating is similar to that found previously for SK2 channels (18, 24). However, diC8-PIP2 exhibits a higher affinity than that found for SK2 channels. Can PIP2 and Ca^{2+} dynamically modulate SK4 channels under physiological conditions? For SK2 channels, it was elegantly shown that phosphorylation by CK2 of residue T79 in the CaM linker reduces the affinity of PIP2 (18). This effect of CaM phosphorylation was shown to promote greater SK2 channel inhibition by G-protein–mediated hydrolysis of PIP2 (18). Our data showed that the phosphomimetic CaM mutant, T79D, markedly lowers the affinity of diC8-PIP2 for SK4 channel activation. Thus, like with SK2 channels, phosphorylation of CaM at T79 can decrease the sensitivity of SK4 channels to PIP2 and Ca^{2+} and thereby potentially tune the dynamic range of actual ligand concentrations required for gating.

The pharmacological toolbox of SK4 channel blockers has mainly focused on targeting the pore region, and currently existing inhibitory drugs do not obviously suit for clinical development (2, 18, 21, 22). In this study, we aimed to target blockers to the SK4 channel gating machinery. Thus, using the 2-benzimidazolinone template, 1-EBIO (23), known to act as a nonselective opener at the CaM-binding domain (24, 25), the BA6b9 molecule was designed to comprise a benzoxazole ring with a carbonyl group and an heptyl tail. Thanks to H-bonding and π–π stacking interactions, BA6b9 docks nearby PIP2 to the CPBD, a specific region located at the boundary of the channel proximal carboxyl terminus and the S4–S5 linker. Remarkably, BA6b9 mainly interacts with R191 and H192, two residues that are not conserved in SK1–SK3 subunits, therefore conferring SK4 channel selectivity. The computational docking clash of the CaM linker region onto BA6b9 with the resulting lower inhibition displayed by mutants M72A and M76A and the rightward shift of the Ca^{2+} dependence for SK4 channel activation suggest that BA6b9 allosterically inhibits SK4 channels. It does so by acting at the CaM–PIP2 interface to disrupt the correct interaction of the calcified CaM *N*-lobe with the proximal $S_{45}A$ helix and, as such, prevents gate opening. Although the interface between the CaM *N*-lobe and the $S_{45}A$ linker helix is reported to be the target of some benzothiazole/oxazole-type SK channel activators (SKA compounds) (31), BA6b9 is, to our knowledge, the first allosteric inhibitor that is rationally designed to act at the CPBD region to prevent opening of the remote channel gate. For example, the KCa channel activator SKA-111 is assumed to bind to the pocket formed by the $S_{45}A$ helix and the CaM *N*-lobe. It interacts with SK4 channel residues S181, A184, and L185 (31), which are conserved in SK1–3 channel subunits, raising the concern of selectivity of such molecules. Advantageously, BA6b9 interacts with the $S_{45}A$ helix at residues R191 and H192 that are not shared by SK1–3 channel subunits, which provides a remarkable selectivity for SK4 channels as confirmed by electrophysiological data. Strengthening this notion of allosteric modulator, the slight modification of the ligand by removing the alkyl chain and substituting the aromatic ring with halogen atoms, such as in BA40 and BA100, converts these molecules to openers. We showed that BA40 and 1-EBIO dock very differently from BA6b9 to the SK4 channel in a way that possibly stabilizes CaM and PIP2 interactions with the S4–S5 linker. Obviously, BA6b9 low solubility in aqueous solutions might not be optimal for drug development, but ongoing experiments are designed to improve its affinity and optimize its solubility.

In the heart, SK1–SK3 channels are mainly expressed in atrial myocytes, where they are activated by increased cytoplasmic Ca^{2+} (26). They are involved in late action potential repolarization in human atria (32). While the role of SK1–SK3 channels in the genesis of cardiac arrhythmias is increasingly documented, it is still not clear what the consequences of their activation or inhibition are (26, 33, 34). Recent studies (13, 14, 29), including our own work (10, 11), suggest that SK4 channel blockers may be of therapeutic potential for treating cardiac arrhythmias. We previously showed that Tram-34 prominently reduces the ECG arrhythmic features of CPVT model mice (10). Another work showed in canine heart that SK4 K^+ channels are expressed in atria and are up-regulated after acute stroke or rapid atrial pacing (14). Here, our immunohistochemistry data also indicate the strong expression of the SK4 channel protein in rat atrium, which is localized to the sarcolemmal membrane and intracellularly in a striated Z-band pattern across the myocytes. This tissue distribution is similar to that described for SK1–SK3 channels in mouse atrial cardiomyocytes (32). In the ventricle, SK4 channels are detected in the sarcolemma and intracellular regions, although at lower intensity than in the atrium, but they additionally localize to intercalated discs, the site of contact between adjacent cardiomyocytes that confers mechanical and electrical cellular coupling. A no. of ion channels are targeted to the intercalated disk membrane structure, such as connexin 43 (Cx43), the Na^+ channel Nav1.5, and K^+ channels, like Kv1.5, Kv7.1, SK2, Kir 6.2, Kir 2.1, or Kir 2.3 (32, 35–37). Although the presence of SK4 channels in intercalated disk membranes suggests a possible involvement in intercellular junctions, their role in this context remains to be elucidated.

Importantly, the present study shows that the allosteric SK4 channel blocker, BA6b9, significantly prolongs AERP and AVERP in healthy rat hearts, with VERP remaining unchanged and hemodynamic parameters only mildly affected. Moreover,

BA6b9 decreases the AF substrate induced by carbachol. Similar features are exhibited by Tram-34. Interestingly, a recent work reported that inhibition of SK4 channels by Tram-34 potently suppresses in vivo the vulnerability to AF induced by rapid atrial pacing in canine heart (29), suggesting that additional animal models of AF need to be examined with BA6b9 in future studies, notably by using primate or porcine hearts that are more similar to those of humans. Of note, the supraventricular impact of SK4 channel blockage, the negative chronotropic and dromotropic effects, useful in AF rate control and hemodynamic stability, all support the notion that blockage of SK4 channels is an attractive pharmacological target for the treatment of AF.

In conclusion, in contrast to classical approaches that target drug blockers to the relatively conserved and hydrophobic pore region of K^+ channels, our strategy to design allosteric inhibitors acting to the specific CaM–PIP2-binding interface may offer a promise for selectivity and, as exemplified by SK4 K^+ channels, a therapeutic opportunity to treat cardiac arrhythmias, such as AF.

Materials and Methods

Constructs. Human SK1, rat SK2, human SK3, and rat CaM into the pcDNA3 vector as well as human SK4 into pEGFP-C1 vector and PIP4,5-kinase into an IRES-dsRed plasmid were used for CHO cell transfection. The mutations were introduced using the PCR-based Quikchange site-directed mutagenesis (Stratagene) and were verified by full sequencing of the entire plasmid vector.

Drugs. Poly L-Lysine 50 μg/mL (PLL hydrochloride, molecular weight [MW] = 8,200 Da (Alamanda Polymers Inc.), PI(4,5)P2 diC8 (dioctanoyl, PIP2; Echelon Biosciences), Tram-34 (Alomone Labs) and carbachol (carbamylcholine chloride; Sigma-Aldrich) were used in this study.

Cell Culture and Transfection. CHO cells were grown in Dulbecco's modified Eagle's medium supplemented with 2 mM glutamine, 10% fetal calf serum, and antibiotics. In brief, 20,000 cells seeded on PLL-coated glass coverslips (13 mm in diameter) in a 24-multiwell plate were transfected with 0.5 μg pEGFP-SK4/0.5 μg mutant SK4, 1.2 μg dsRed-PIP4,5K, or with 1 μg SK1/SK2/SK3 together with pIRES-CD8 (0.3 μg) as a marker for transfection. Transfection was performed using TransIT-LT1 Transfection Reagent (Mirus Bio) according to the manufacturer's protocol. For electrophysiology, transfected cells were visualized ∼40 h after transfection with a Zeiss Axiovert 35 inverted florescence microscope.

The experimental procedures for recombinant expression and purification of CaM, electrophysiology, immunostaining, medicinal chemistry, computational methods, and ex vivo experiments are detailed in the *SI Appendix*.

Data, Materials, and Software Availability. All data are included in the manuscript and/or *SI Appendix*.

All study data are included in the article and/or supporting information.

ACKNOWLEDGMENTS. This work was supported by grants from the Israel Science Foundation (ISF 3129/21, to B.A.) and Israel Innovation Authority (Kamin-69124, to B.A. and Y.E.). B.A. holds the Andy Libach Professorial Chair in clinical pharmacology and toxicology. We thank Dr. Heike Wulff (Department of Pharmacology, University of California, Davis, CA) and Dr. Anastasios V. Tzingounis (Department of Physiology and Neurobiology, University of Connecticut, Storrs, CT) for their kind gift of human SK4 channel and PIP4,5-kinase plasmids, respectively.

Author affiliations: [a]Department of Physiology & Pharmacology, Tel Aviv University, Tel Aviv 69978, Israel; [b]Cardiac Arrhythmia Research Laboratory, Department of Physiology and Cell Biology, Faculty of Health Sciences, Regenerative Medicine & Stem Cell Research Center, Ben-Gurion University of the Negev, Beer-Sheva, 8410501, Israel; [c]The Blavatnik Center for Drug Discovery, Tel Aviv University, Tel Aviv 69978, Israel; [d]The Laboratory of Structural Physiology of the Sackler Faculty of Medicine and Sagol School of Neurosciences, Tel Aviv University, Tel Aviv 69978, Israel; and [e]Regenerative Medicine & Stem Cell Research Center, Ben-Gurion University of the Negev, Beer-Sheva, 8410501, Israel

1. H. Berkefeld, B. Fakler, U. Schulte, Ca^{2+}-activated K^+ channels: From protein complexes to function. *Physiol. Rev.* **90**, 1437–1459 (2010).
2. B. M. Brown, H. Shim, P. Christophersen, H. Wulff, Pharmacology of small- and intermediate-conductance calcium-activated potassium channels. *Annu. Rev. Pharmacol. Toxicol.* **60**, 219–240 (2020).
3. L. Sforna, A. Megaro, M. Pessia, F. Franciolini, L. Catacuzzeno, Structure, gating and basic functions of the Ca^{2+}-activated K channel of intermediate conductance. *Curr. Neuropharmacol.* **16**, 608–617 (2018).
4. C. H. Lee, R. MacKinnon, Activation mechanism of a human SK-calmodulin channel complex elucidated by cryo-EM structures. *Science* **360**, 508 (2018).
5. M. D. Cahalan, K. G. Chandy, The functional network of ion channels in T lymphocytes. *Immunol. Rev.* **231**, 59–87 (2009).
6. S. Feske, H. Wulff, E. Y. Skolnik, Ion channels in innate and adaptive immunity. *Annu. Rev. Immunol.* **33**, 291–353 (2015).
7. H. Wulff, R. Köhler, Endothelial small-conductance and intermediate-conductance KCa channels: An update on their pharmacology and usefulness as cardiovascular targets. *J. Cardiovasc. Pharmacol.* **61**, 102–112 (2013).
8. J. D. Engbers *et al.*, Intermediate conductance calcium-activated potassium channels modulate summation of parallel fiber input in cerebellar Purkinje cells. *Proc. Natl. Acad. Sci. U.S.A.* **109**, 2601–2606 (2012).
9. B. King *et al.*, IKCa channels are a critical determinant of the slow AHP in CA1 pyramidal neurons. *Cell Rep.* **11**, 175–182 (2015).
10. S. Haron-Khun *et al.*, SK4 K^+ channels are therapeutic targets for the treatment of cardiac arrhythmias. *EMBO Mol. Med.* **9**, 415–429 (2017).
11. D. Weisbrod *et al.*, SK4 Ca^{2+} activated K^+ channel is a critical player in cardiac pacemaker derived from human embryonic stem cells. *Proc. Natl. Acad. Sci. U.S.A.* **110**, E1685–E1694 (2013).
12. H. Nouchi *et al.*, Chronic left atrial volume overload abbreviates the action potential duration of the canine pulmonary vein myocardium via activation of IK channel. *Eur. J. Pharmacol.* **597**, 81–85 (2008).
13. M. Yang *et al.*, SK4 calcium-activated potassium channels activated by sympathetic nerves enhances atrial fibrillation vulnerability in a canine model of acute stroke. *Heliyon* **6**, e03928 (2020).
14. M. Yang *et al.*, Role of intermediate-conductance calcium-activated potassium channels in atrial fibrillation in canines with rapid atrial pacing. *J. Interv. Card Electrophysiol.* **60**, 247–253 (2021).
15. W. J. Joiner, L. Y. Wang, M. D. Tang, L. K. Kaczmarek, hSK4, a member of a novel subfamily of calcium-activated potassium channels. *Proc. Natl. Acad. Sci. U.S.A.* **94**, 11013–11018 (1997).
16. W. J. Joiner, R. Khanna, L. C. Schlichter, L. K. Kaczmarek, Calmodulin regulates assembly and trafficking of SK4/IK1 Ca^{2+}-activated K^+ channels. *J. Biol. Chem.* **276**, 37980–37985 (2001).
17. C. M. Lopes *et al.*, PIP2 hydrolysis underlies agonist-induced inhibition and regulates voltage gating of two-pore domain K^+ channels. *J. Physiol.* **564**, 117–129 (2005).
18. M. Zhang *et al.*, Selective phosphorylation modulates the PIP2 sensitivity of the CaM-SK channel complex. *Nat. Chem. Biol.* **10**, 753–759 (2014).
19. J. Myeong *et al.*, Phosphatidylinositol 4,5-bisphosphate is regenerated by speeding of the PI 4-kinase pathway during long PLC activation. *J. Gen. Physiol.* **152**, e202012627 (2020).
20. D. Allen, B. Fakler, J. Maylie, J. P. Adelman, Organization and regulation of small conductance Ca^{2+}-activated K^+ channel multiprotein complexes. *J. Neurosci.* **27**, 2369–2376 (2007).
21. B. M. Brown, B. Pressley, H. Wulff, KCa3.1 channel modulators as potential therapeutic compounds for glioblastoma. *Curr. Neuropharmacol.* **16**, 618–626 (2018).
22. H. Wulff, G. A. Gutman, M. D. Cahalan, K. G. Chandy, Delineation of the clotrimazole/TRAM-34 binding site on the intermediate conductance calcium-activated potassium channel, IKCa1. *J. Biol. Chem.* **276**, 32040–32045 (2001).
23. D. C. Devor, A. K. Singh, R. A. Frizzell, R. J. Bridges, Modulation of Cl- secretion by benzimidazolones. I. Direct activation of a Ca^{2+}-dependent K^+ channel. *Am. J. Physiol.* **271**, L775–L784 (1996).
24. M. Zhang, X. Y. Meng, J. F. Zhang, M. Cui, D. E. Logothetis, Molecular overlap in the regulation of SK channels by small molecules and phosphoinositides. *Sci. Adv.* **1**, e1500008 (2015).
25. M. Zhang, J. M. Pascal, M. Schumann, R. S. Armen, J. F. Zhang, Identification of the functional binding pocket for compounds targeting small-conductance Ca^{2+}-activated potassium channels. *Nat. Commun.* **3**, 1021 (2012).
26. L. Crotti, K. E. Odening, M. C. Sanguinetti, Heritable arrhythmias associated with abnormal function of cardiac potassium channels. *Cardiovasc. Res.* **116**, 1542–1556 (2020).
27. E. Grandi *et al.*, Potassium channels in the heart: Structure, function and regulation. *J. Physiol.* **595**, 2209–2228 (2017).
28. U. Ravens, K. E. Odening, Atrial fibrillation: Therapeutic potential of atrial K^+ channel blockers. *Pharmacol. Ther.* **176**, 13–21 (2017).
29. S. He *et al.*, Inhibition of KCa3.1 channels suppresses atrial fibrillation via the attenuation of macrophage pro-inflammatory polarization in a canine model with prolonged rapid atrial pacing. *Front. Cardiovasc. Med.* **8**, 656631 (2021).
30. H. Wulff *et al.*, Design of a potent and selective inhibitor of the intermediate-conductance Ca2+-activated K+ channel, IKCa1: A potential immunosuppressant. *Proc. Natl. Acad. Sci. U.S.A.* **97**, 8151–8156 (2000).
31. H. Shim *et al.*, The trials and tribulations of structure assisted design of K_{Ca} channel activators. *Front. Pharmacol.* **10**, 972 (2019).
32. L. Skibsbye *et al.*, Small-conductance calcium-activated potassium (SK) channels contribute to action potential repolarization in human atria. *Cardiovasc. Res.* **103**, 156–167 (2014).
33. S. Burg, B. Attali, Targeting of potassium channels in cardiac arrhythmias. *Trends Pharmacol. Sci.* **42**, 491–506 (2021).
34. N. Chiamvimonvat *et al.*, Potassium currents in the heart: Functional roles in repolarization, arrhythmia and therapeutics. *J. Physiol.* **595**, 2229–2252 (2017).
35. M. Hong *et al.*, Heterogeneity of ATP-sensitive K^+ channels in cardiac myocytes: Enrichment at the intercalated disk. *J. Biol. Chem.* **287**, 41258–41267 (2012).
36. D. J. Mays, J. M. Foose, L. H. Philipson, M. M. Tamkun, Localization of the Kv1.5 K^+ channel protein in explanted cardiac tissue. *J. Clin. Invest.* **96**, 282–292 (1995).
37. P. Melnyk *et al.*, Comparison of ion channel distribution and expression in cardiomyocytes of canine pulmonary veins versus left atrium. *Cardiovasc. Res.* **65**, 104–116 (2005).